MESSENGER observations of dipolarization events in Mercury's magnetotail

Torbjörn Sundberg,[1] James A. Slavin,[2] Scott A. Boardsen,[1,3] Brian J. Anderson,[4] Haje Korth,[4] George C. Ho,[4] David Schriver,[5,6] Vadim M. Uritsky,[1,7] Thomas H. Zurbuchen,[2] Jim M. Raines,[2] Daniel N. Baker,[8] Stamatios M. Krimigis,[4,9] Ralph L. McNutt Jr.,[4] and Sean C. Solomon[10,11]

Received 23 March 2012; revised 5 July 2012; accepted 11 July 2012; published 6 September 2012.

[1] Several series of large dipolarization events are documented from magnetic field observations in Mercury's magnetotail made by the MESSENGER spacecraft. The dipolarizations are identified by a rapid (~1 s) increase in the northward component of the magnetic field, followed by a slower return (~10 s) to pre-onset values. The changes in field strength during an event frequently reach 40 nT or higher, equivalent to an increase in the total magnetic field magnitude by a factor of ~4 or more. The presence of spatially constrained dipolarizations at Mercury provides a key to understanding the magnetic substorm process in a new parameter regime: the dipolarization timescale, which is shorter than at Earth, is suspected to lead to efficient non-adiabatic heating of the plasma sheet proton population, and the high recurrence rate of the structures is similar to that frequently observed for flux ropes and traveling compression regions in Mercury's magnetotail. The relatively short lifetime of the events is attributed to the lack of steady field-aligned current systems at Mercury.

Citation: Sundberg, T., et al. (2012), MESSENGER observations of dipolarization events in Mercury's magnetotail, *J. Geophys. Res.*, *117*, A00M03, doi:10.1029/2012JA017756.

1. Introduction

[2] Recent observations by the MErcury Surface, Space ENvironment, GEochemistry, and Ranging (MESSENGER) spacecraft have confirmed and broadened our view of Mercury's magnetosphere as a complex and dynamic system, in part due to the extreme solar wind conditions encountered in the inner solar system. Phenomena at Mercury analogous to a number of features of the terrestrial magnetosphere have already been observed by MESSENGER, including reconnection at the dayside magnetopause, flux transfer events, plasmoid ejection, Kelvin-Helmholtz waves, and magnetotail loading–unloading cycles [e.g., *Slavin et al.*, 2009, 2010, 2012; *Sundberg et al.*, 2012]. The planet possesses a relatively weak magnetic dipole moment (195 nT R_M^{-3}, where R_M is Mercury's radius or 2440 km), aligned to within 3° of the rotational axis of the planet, although displaced ~0.2 R_M north of the planetary center [*Anderson et al.*, 2011]. Together with the strong interplanetary magnetic field (IMF) at Mercury's orbit, the weak internal field yields a magnetosphere heavily dominated by reconnection: the ratio of the normal magnetic field component to the total field at the dayside magnetopause frequently reaches 0.5, indicating a reconnection efficiency almost a factor of 10 higher than at Earth [*Slavin et al.*, 2009; G. A. DiBraccio et al., MESSENGER observations of magnetopause structure and dynamics at Mercury, submitted to *Journal of Geophysical Research*, 2012]. Altogether, these observations have established Mercury's magnetosphere as driven primarily by a Dungey cycle [e.g., *Dungey*, 1961] with an approximate loading–unloading period of 2–3 min [*Slavin et al.*, 2010]. When the IMF is predominantly southward, however, the behavior resembles the steady magnetospheric convection

[1]Heliophysics Science Division, NASA Goddard Space Flight Center, Greenbelt, Maryland, USA.
[2]Department of Atmospheric, Oceanic and Space Sciences, University of Michigan, Ann Arbor, Michigan, USA.
[3]Goddard Earth Sciences and Technology Center, University of Maryland, Baltimore County, Baltimore, Maryland, USA.
[4]Johns Hopkins University Applied Physics Laboratory, Laurel, Maryland, USA.
[5]Institute of Geophysics and Planetary Physics, University of California, Los Angeles, California, USA.
[6]Department of Physics and Astronomy, University of California, Los Angeles, California, USA.
[7]Department of Physics, Catholic University of America, Washington, D. C., USA.
[8]Laboratory for Atmospheric and Space Physics, University of Colorado Boulder, Boulder, Colorado, USA.
[9]Academy of Athens, Athens, Greece.
[10]Department of Terrestrial Magnetism, Carnegie Institution of Washington, Washington, D. C., USA.
[11]Lamont-Doherty Earth Observatory, Columbia University, Palisades, New York, USA.

Corresponding author: T. Sundberg, Heliophysics Science Division, NASA Goddard Space Flight Center, Greenbelt, MD 20771, USA. (torbjorn.sundberg@nasa.gov)

0148-0227/12/2012JA017756

events seen at Earth [e.g., *Sergeev et al.*, 1990, 1996a; *Kissinger et al.*, 2012] rather than the loading–unloading cycle typically expected. Periods of strong loading and unloading, such as those observed during MESSENGER's third Mercury flyby [*Slavin et al.*, 2010], have instead been interpreted as a consequence of a temporally varying IMF [*Slavin et al.*, 2012].

[3] One of the open issues regarding magnetotail dynamics that remains is whether global or local Earth-like substorms, a consequence of explosive nightside reconnection [e.g., *Baker et al.*, 1996], tend to develop in Mercury's magnetotail. Possible diagnostics are localized, sunward-traveling, high-speed and low-density plasma streams in the central plasma sheet, known as bursty bulk flows (BBFs) [e.g., *Baumjohann et al.*, 1990; *Angelopoulos et al.*, 1992, 1994; *Sergeev et al.*, 1996b; *Sergeev*, 2004; *Raj et al.*, 2002; *Li et al.*, 2011]. At Earth, such regions of strongly enhanced plasma convection are frequently observed during active periods and are often accompanied by dipolarizations – rapid, large-amplitude increases in the northward component of the magnetic field **B** that change the stretched tail field into a more dipolar configuration [e.g., *Angelopoulos et al.*, 1992], as well as field-aligned current systems on the dawn- and duskward edges of the flow channel [*Angelopoulos et al.*, 1997; *Kauristie et al.*, 2000; *Nakamura et al.*, 2001, 2004; *Grocott et al.*, 2004; *Keiling et al.*, 2009]. The earthward-propagating dipolarization fronts are usually accompanied by an increase in high-energy ion and electron fluxes with energies up to hundreds of keV [*Runov et al.*, 2009; *Asano et al.*, 2010; *Ashour-Abdalla et al.*, 2011].

[4] Two possible dipolarization events were reported from measurements made during Mariner 10's first Mercury flyby (MI) [*Eraker and Simpson*, 1986; *Baker et al.*, 1986; *Christon et al.*, 1987]. The observed magnetic field signatures were in good agreement with those expected from terrestrial dipolarization events. The fact that no supporting observations were seen during the MESSENGER flybys, however, or during the spacecraft's early period in orbit raised doubts about whether Earth-like substorms with explosive nightside reconnection, high-speed plasma sheet flows, and associated dipolarization fronts in the magnetic field are supported by Mercury's magnetosphere, especially given the lack of signatures of field-aligned currents (FACs) at Mercury.

[5] We here further investigate the nature of magnetotail dynamics at Mercury through a systematic survey of MESSENGER magnetotail observations, and we present multiple examples of repeated magnetic field dipolarization events in the near-tail plasma sheet. The observations provide strong evidence for substorm-like behavior of the magnetotail, possibly related to spatially constrained flow channels and efficient heating of electrons and light ions.

2. Instrumentation and Data

[6] MESSENGER successfully performed its orbit insertion around Mercury on 18 March 2011, and it has since then been providing continuous in situ measurements from the planetary environment. Here we focus on data collected by the Magnetometer (MAG) instrument [*Anderson et al.*, 2007] and the Energetic Particle and Plasma Spectrometer (EPPS) [*Andrews et al.*, 2007]. The EPPS consists of two separate sensors: the Energetic Particle Spectrometer (EPS), which measures high-energy electrons and ions, and the Fast Imaging Plasma Spectrometer (FIPS), which measures thermal and low-energy ions for ratios of energy per charge q between <50 eV/q and 13 keV/q. The sampling periods of MAG, EPS, and FIPS are 0.05 s, 3 s, and 8 s, respectively. During its primary orbital mission, MESSENGER followed a highly eccentric orbit with periapsis and apoapsis distances of $\sim$1.1 R_M and $\sim$7 R_M from the center of the planet, respectively. The orbit was inclined 82.5° to Mercury's orbital plane, and the initial periapsis latitude was 60°N. The longitude of the orbital axis progressed around the planet over the Mercury year, completing one full lap every 88 days, so the spacecraft crossed the equatorial magnetotail at two radial distances from the dipole center: $\sim$(1.3–1.4) R_M and $\sim$(2.5–2.6) R_M during the short-tail and long-tail seasons of 2011, respectively [*Solomon et al.*, 2001].

[7] To portray the magnetospheric dynamics clearly, we here utilize the Mercury solar magnetospheric (MSM) coordinate system centered at the origin of the planetary dipole, 484 km north of the planetary center [*Anderson et al.*, 2011]. In MSM coordinates, the X-axis is directed toward the Sun, and the Z-axis is in the direction of magnetic north, which is normal to Mercury's orbital plane and in the direction of the north celestial pole. The Y-axis is positive toward dusk and completes the right-handed X, Y, Z system.

3. Observations and Analysis

[8] At Earth, bursty bulk flows have been characterized as bursts of enhanced plasma convection with a peak velocity exceeding 400 km/s [*Angelopoulos et al.*, 1992] or, similarly, periods of increased earthward flux transport at rates exceeding $\sim$10 times the average magnetotail convection flux [*Schödel et al.*, 2001; *Sergeev*, 2004]. Although these high-speed flows cannot be observed by MESSENGER because of obstructions to the field of view of FIPS by the spacecraft sunshade, thermal constraints on spacecraft pointing, and the time resolution of the phenomena, the associated magnetic field dipolarization can be directly measured by the Magnetometer. It should be noted that although there is not a strict one-to-one correspondence between dipolarization events and bursty bulk flows, there is generally good agreement between the two in terrestrial measurements [*Angelopoulos et al.*, 1992; *Lee et al.*, 2012].

[9] We performed a visual survey of the equatorial magnetotail data collected between 22 March and 31 December 2011, in search of sharp and repeated step-like increases in the B_z component of the magnetic field followed by a gradual reduction to pre-onset values, characteristic of dipolarization fronts. The time period analyzed incorporates four short-tail and two long-tail seasons of the orbit. (The scientific instruments were not operated during the first long-tail season because of concern over high spacecraft temperatures on the dayside.) Although the overall topology of the magnetospheric field configuration is in general well-described by the model of *Alexeev et al.* [2008, 2010], the magnetic field behavior in the plasma sheet cannot be adequately reproduced by the model because the equatorial magnetotail crossings often are marked by substantial magnetic depressions caused by the relatively high plasma pressure, on average 0.1–0.3 nPa [*Korth et al.*, 2011; *Raines*

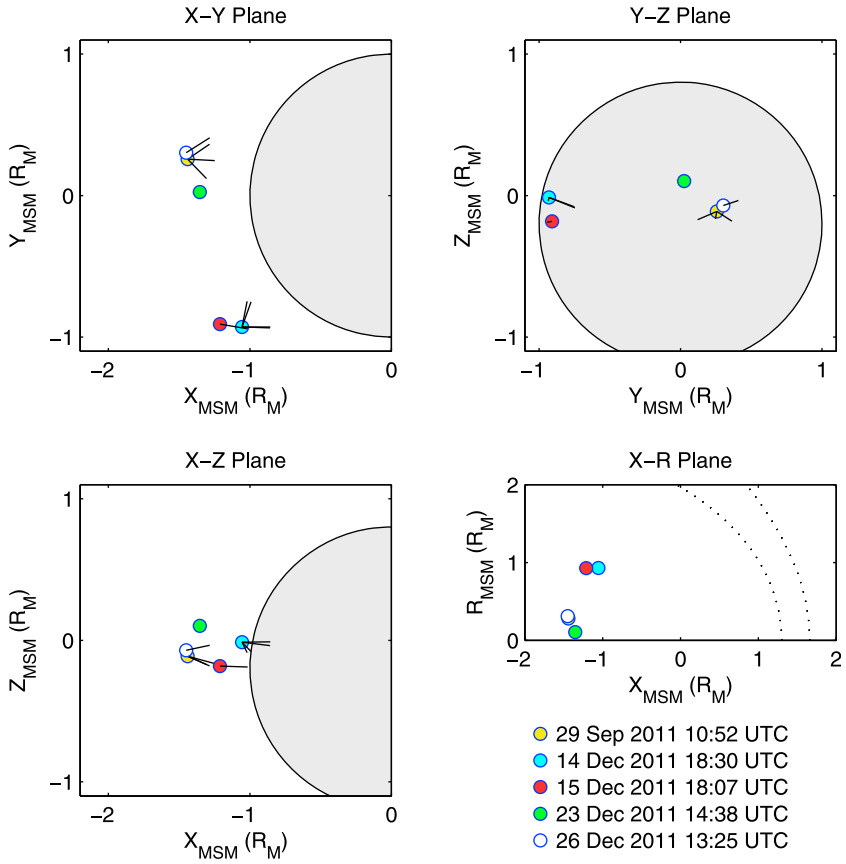

Figure 1. Location of the observed dipolarization events in Table 1. The colored circles show the spacecraft position at the center of the plasma sheet crossing. Projections onto the (top left) $Z = 0$, (top right) $X = 0$, and (bottom left) $Y = 0$ planes. (bottom right) The radial distance $R = (X^2 + Y^2)^{0.5}$ from the X-axis. Solid lines show the projections of the current-sheet normals given in Table 2.

et al., 2011]. (These pressures correspond to a plasma β, the ratio between the plasma and magnetic pressure, of ~1–10.)

[10] As the plasma sheet is characterized by highly variable magnetic fields, often associated with wave activity [*Schriver et al.*, 2011; *Boardsen et al.*, 2012], reliable determination of dipolarization events is difficult, especially given the short spacecraft transit time through the region, typically ~5 min.

[11] Evidence for recurring dipolarization structures was found on three occasions: 29 September, 14 December, and 15 December 2011. These series of events allowed us to determine and categorize the magnetic field signatures of dipolarization events at Mercury. With that knowledge two additional events were identified on 23 and 26 December (Figure 1). These two plasma sheet crossings were isolated events and did not show the same pattern of repeated dipolarizations. All events were observed inside the plasma sheet during short-tail crossings, very close to the magnetic equatorial plane, in either the central or the dawn-side magnetotail, as shown in Figure 1.

[12] Given the sparse set of observations we make no conclusion regarding any dawn-dusk difference in the occurrence rates. A summary of the identified event periods is given in Table 1, together with an overview of the IMF conditions observed before and after the inbound and outbound bow shock crossings, respectively. However, as there is a time lag of an hour or more between plasma sheet and IMF observations, the conditions given should be interpreted with caution and are here used solely as an indication of overall interplanetary conditions. The 3-s-resolution electron data from the EPS instrument show the presence of high-energy electrons during the time periods of interest but no substantial fluxes of high-energy ions. However, the energetic electrons are little correlated with the individual dipolarization events, in contrast to what was reported for the events seen by Mariner 10 [e.g., *Christon et al.*, 1987].

Table 1. Observed Dipolarization Events at Mercury[a]

Year	Day	Time (UTC)	Dipolarizations	Upstream B_z	Downstream B_z
2011	29 Sep	10:49–10:57	10	-6 ± 7 nT	-2 ± 6 nT
2011	14 Dec	18:25–18:33	7	4 ± 11 nT	-5 ± 11 nT
2011	15 Dec	18:04–18:10	5	1 ± 7 nT	4 ± 4 nT
2011	23 Dec	14:37–14:44	1	-17 ± 5 nT	-1 ± 8 nT
2011	26 Dec	13:23–13:28	1	-1 ± 11 nT	-5 ± 7 nT

[a]Included are the time interval of the plasma sheet crossing, the number of clear dipolarizations observed during this interval, and the upstream and downstream IMF B_z component observed by the spacecraft before and after the inbound and outbound crossings of the bow shock, respectively. The IMF values given are 15-min mean values together with their respective standard deviations. All IMF measurements were made at times more than 1 h before or after the dipolarization events and should therefore be regarded as only approximate indicators of interplanetary conditions at the specific event times.

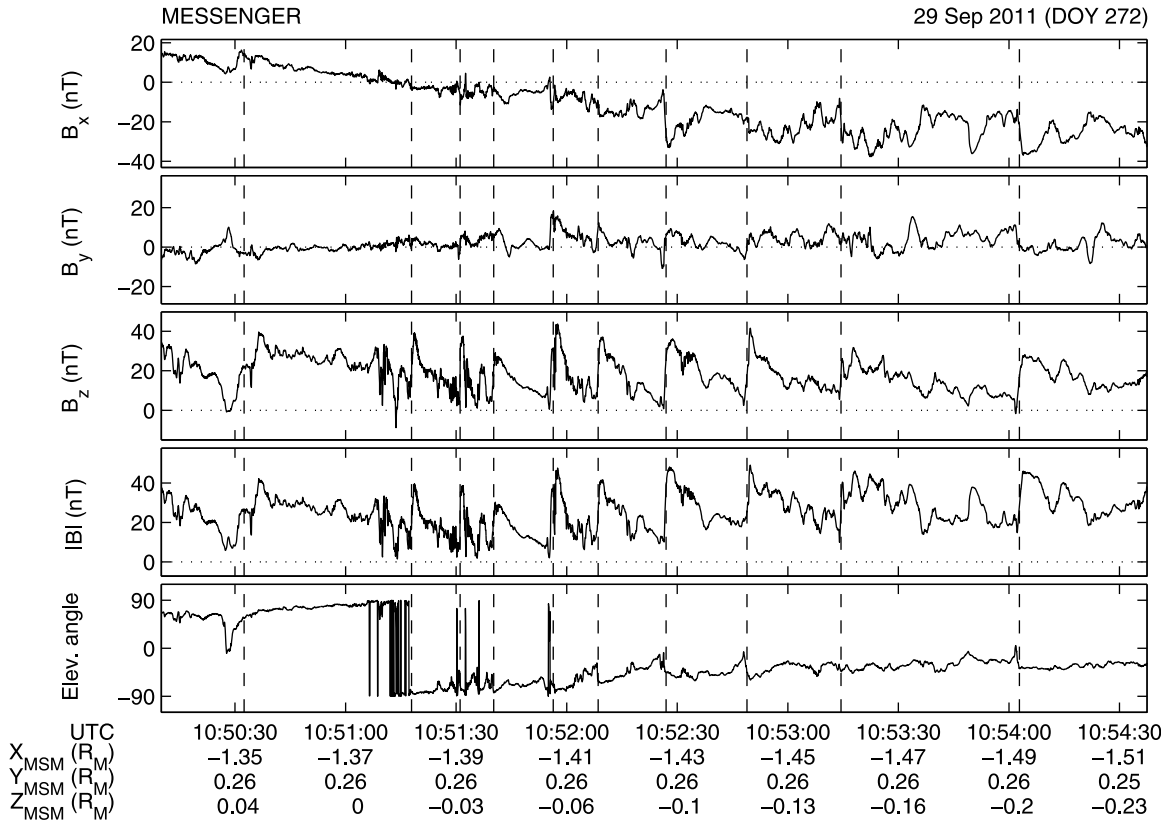

Figure 2. Overview of Magnetometer measurements during a plasma sheet crossing on 29 September 2011. The panels show, from top to bottom, the *X*, *Y*, and *Z* components of the magnetic field; the field magnitude; and the elevation angle, $\tan^{-1}(B_z/B_x)$. The dashed lines mark a series of 10 dipolarization events observed in the magnetic field over a period of 4 min. DOY stands for day of the year.

[13] Also, MESSENGER's X-Ray Spectrometer (XRS) instrument, which can serve as a proxy for the presence of 1–10 keV electrons [*Slavin et al.*, 2008; *Ho et al.*, 2011], recorded a time-varying electron population during the same time intervals. However, the presence of 1–10 keV electrons is not restricted to the dipolarization events listed, since in the nightside plasma sheet region near the geomagnetic equator such an electron population is commonly observed over a wide range of local times around Mercury [*Schriver et al.*, 2011], and because of the coarse time resolution of the XRS detection signal it cannot be determined if there are correlations of the electrons with each dipolarization front.

[14] An overview of one of the event periods, on 29 September, is shown in Figure 2. Clear consecutive dipolarization signatures, marked by dashed lines, are seen in the B_z component of the magnetic field. Each event is characterized by a sharp increase of up to 40–50 nT in the field strength over a period of ~1 s followed by a slower decrease (~10 s) back toward the baseline value. For several of the events in Figure 2, the magnetic field exhibits bursty features similar to those observed during both the event seen by Mariner 10 and terrestrial analogue events [e.g., *Christon et al.*, 1987; *Ohtani et al.*, 2004; *Sigsbee et al.*, 2005; *Schmid et al.*, 2011; *Runov et al.*, 2011]. We focus here on events that have clear and isolated signatures. Several additional events possibly associated with dipolarizations are present during the plasma sheet crossing, but because of a slower initial response and/or lower magnitude of the increase, we cannot make a fully reliable classification of these intervals. The temporal spacing of the events in the clear dipolarization sequences varies between 9 and 49 s; the recurrence rate is shortest near the equatorial plane, suggesting a possible location bias in the observation probability linked to a limited spatial extent in the *Z* direction of the structures. The recurrence rate is generally in good agreement with that previously reported for plasmoids and traveling compression regions [*Slavin et al.*, 2012].

[15] A closer view of four dipolarization events is shown in Figure 3, presented in minimum variance coordinate systems defined around the dipolarization front [e.g., *Sonnerup and Scheible*, 1998]. Two features stand out in the data: there is a localized 10–15 nT feature in the direction of intermediate variance just before the dipolarization that lasts on the order of 1 s, and a local minimum in the absolute and/or maximum variance component of the field. As both of these features have been reported for terrestrial BBFs, this observation supports our interpretation [e.g., *Sergeev et al.*, 1996b; *Runov et al.*, 2009]. An overview of the dipolarization timescale, the recovery timescale, and the approximate magnetic field change over the dipolarization front for all of the events included in Table 1 is given in Figures 4 and 5, and a superposed epoch plot of the maximum variance component of all events is given in Figure 6. The dipolarizations are associated with a mean magnetic field increase of 46 nT over a timescale of ~1–2 s (comparable to ~0.1–1

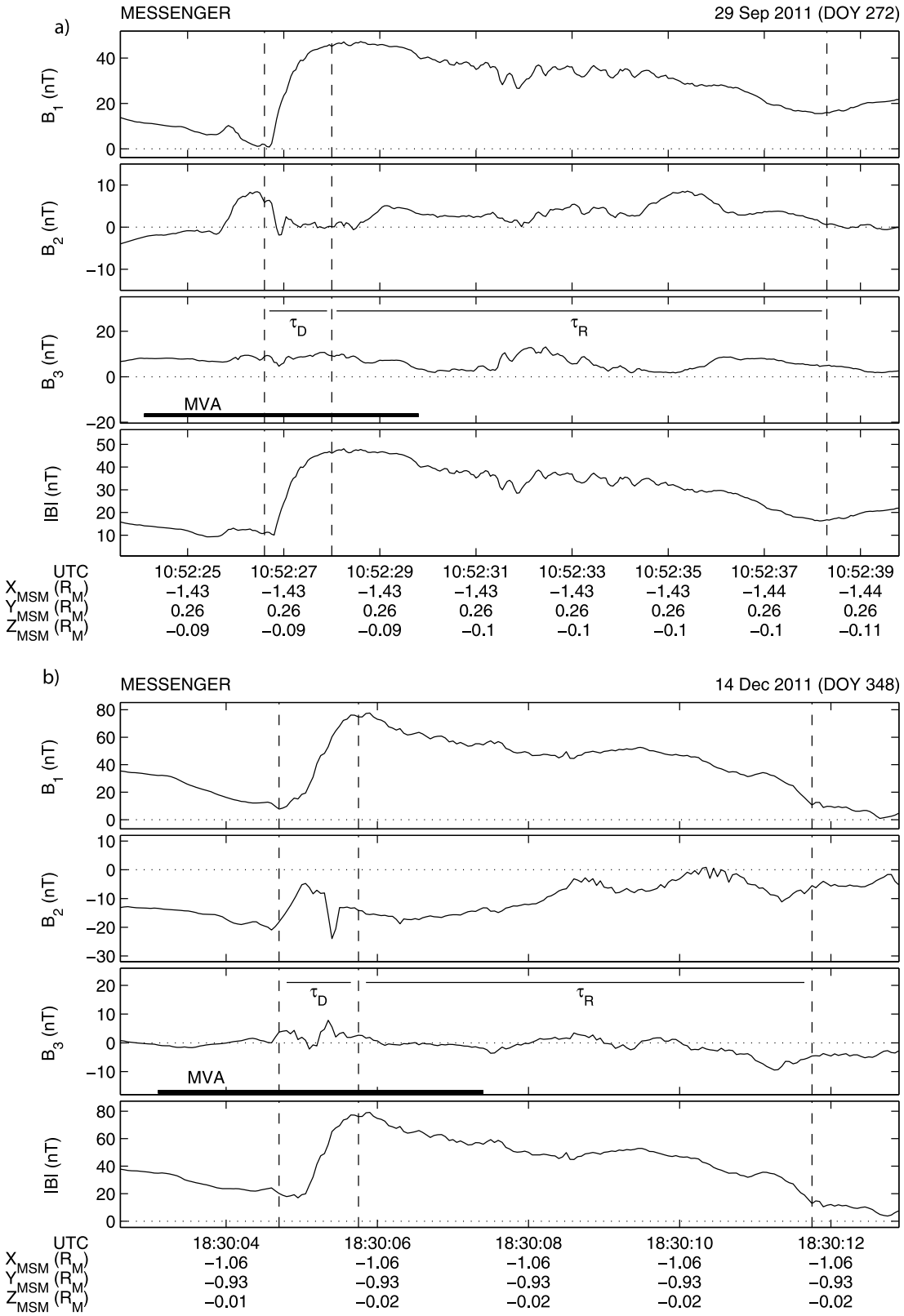

Figure 3. Expanded views of four of the dipolarization events. Each event is displayed in their respective maximum (B_1), intermediate (B_2), and minimum (B_3) variance coordinates as specified in Table 2; the bold line marks the interval over which MVA analysis was performed. The vertical dashed lines give approximate start and end times for the dipolarization and recovery intervals, marked by τ_D and τ_R, respectively. A 10–15 nT disturbance can be clearly seen in the intermediate variance component just before the main field increase in all four events.

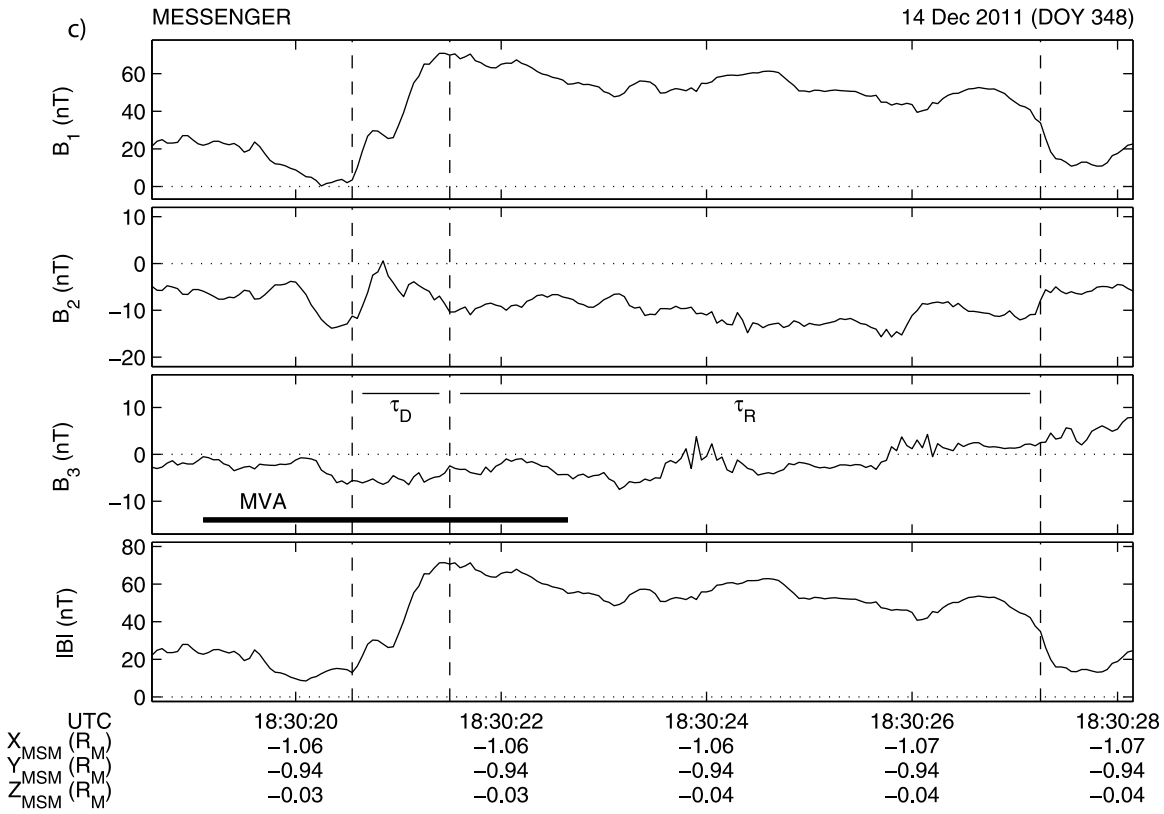

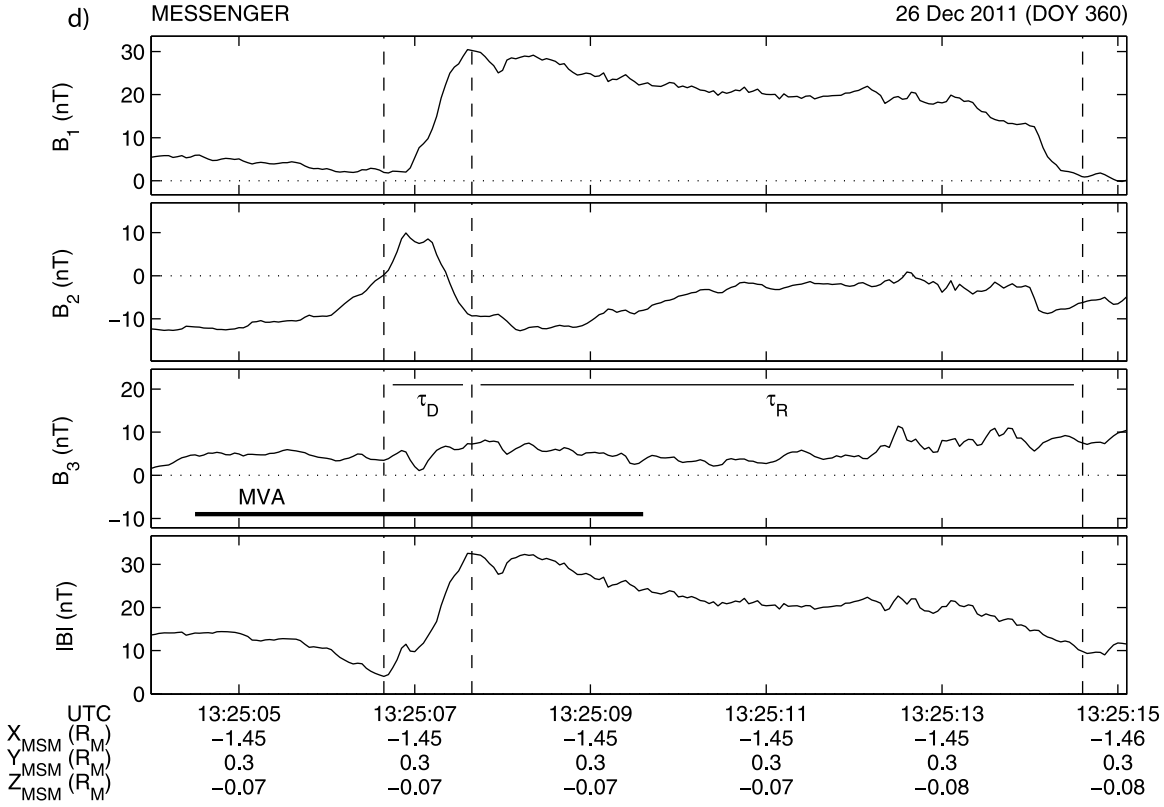

Figure 3. (continued)

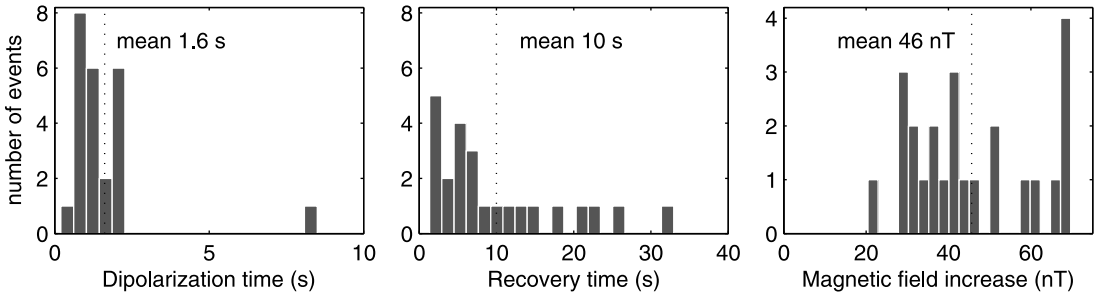

Figure 4. Histograms showing approximate timescales of the dipolarization front, the recovery region, and the magnetic field increase for the events listed in Table 1. Dashed lines mark mean values.

H^+ ion cyclotron periods), with one-third of the events having a risetime of less than 1 s. The recovery phase takes place over ~10 s on average, with the briefest event having a duration of 1.3 s, and the longest ~30 s. Figure 5 also shows a tendency for the quick dipolarizations to be associated with a quicker recovery and a larger increase in the magnetic field than those with a longer rise time.

[16] Out of the plasma sheet crossings presented in Table 1, we selected nine individual events for which the signature and the characteristics of the dipolarization are clear in the directions of both maximum and intermediate variance and deemed adequate for further analysis. Table 2 gives an overview of the maximum (n_1), intermediate (n_2), and minimum (n_3) variance eigenvectors taken over the dipolarization front for each of the selected events, together with the ratios of maximum to intermediate (λ_1/λ_2) and intermediate to minimum eigenvalues (λ_2/λ_3) and the angle α between the projection onto the *X*-*Y* plane of the minimum variance direction and the MSM *X*-axis. It can be seen that the maximum variance direction is well aligned with the MSM *Z*-axis for most of the events, as would be expected from dipolarization. The high λ_1/λ_2 ratios also show that the primary axis is well determined, in that ratios far exceed the conventional limit (for small data sets a λ_1/λ_2 ratio above 10 is usually considered sufficient for adequate determination of the maximum variance direction, and a similar ratio for λ_2/λ_3 yields good determination of the minimum variance direction [e.g., *Sonnerup and Scheible*, 1998]). The ratios associated with the minimum variance direction tend to be low for these events, but because the selected events show a clear disturbance in the B_2 component preceding the dipolarization, we regard the general direction of the current-sheet orientation at the location of the spacecraft crossing as adequately determined.

[17] Qualitative estimates of the spatial topology of each dipolarization feature can be derived from the angle, α, between the *X* direction and the projection of the current-sheet normal at the edge of the dipolarization mapped onto the equatorial plane [e.g., *Sergeev et al.*, 1996b; *Li et al.*, 2011]. A low value of α means that the spacecraft crossed the leading edge of the flow channel, whereas if α deviates markedly from 0° the crossing took place on the flank of the flow region, as illustrated in Figure 7. Negative values of α correspond to a structure passing on the duskward side of the spacecraft, and positive α to the dawnward side. The observation of current-sheet normals that deviate substantially from the MSM *X* direction is a clear sign that the cross-tail scale of the flow channels is spatially constrained. This outcome is particularly well illustrated by the dipolarization event measured on 29 September at 10:51:31 UTC, for which the λ_2/λ_3 ratio was >5 and $|\alpha|$ exceeded 45°. Two dipolarization events on 14 December recorded high values of α, exceeding 70°. Both of these events were among the shortest observed, with the magnetic field impulse receding to pre-onset values about 2 s after the peak response. This duration agrees with the indications from the analysis of current-sheet normal directions that MESSENGER passed through only the outermost edge of the flow region. The analysis gives little information on the actual cross-tail scale of the feature, but an appropriate scaling of terrestrial values gives a spatial extent of about 0.25–0.5 R_M [*Uritsky et al.*, 2011].

[18] *Sergeev et al.* [1996b] used two additional proxies to determine the predominant location of BBFs: the dawn-dusk

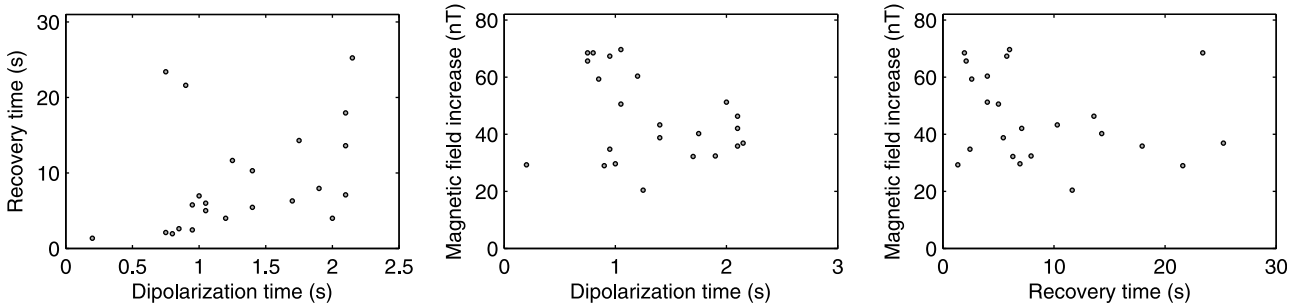

Figure 5. Relations between the dipolarization rise time, the recovery time, and the initial magnetic field increase for the events listed in Table 1. One event with a dipolarization time of 8.5 s, recovery time of 33 s, and magnetic field increase of 42 nT is not shown.

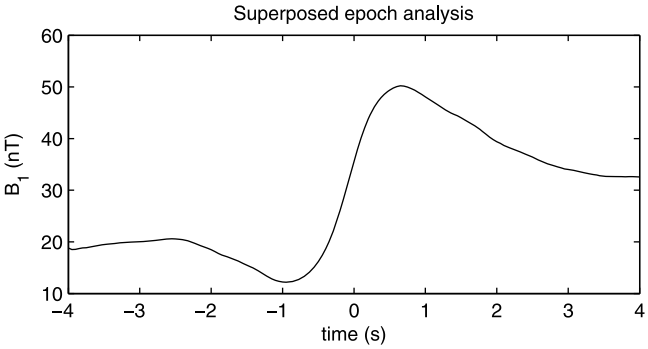

Figure 6. Superposed epoch plot of the maximum variance component for all events listed in Table 1. The timescale covers ±4 s around the center of each dipolarization.

component of the convection velocity, V_y, and the sign of B_x δB_y, where δB_y is the perturbation of the B_y component in the flow shear layer. Their analysis showed good agreement among all three methods, and as the B_x component was close to zero for most of our events and the plasma flow direction is unknown to us, we here rely exclusively on the angle α for analysis.

4. Discussion

[19] The repeated observation of clear B_z-aligned step-like features in the equatorial plane, together with the recurring dip in the magnetic field magnitude just before the onset and the coincident deviations in the intermediate component of the magnetic field (primarily B_y), provides evidence for dipolarization events, possibly associated with bursty bulk flows at Mercury. Together, these features help to distinguish the observed events from other wave-like processes or fluctuations in the plasma sheet density. At Earth, these regions of strongly enhanced plasma convection are frequently observed during active periods, and even though the BBFs are present only ∼5% of the time, they are believed to be responsible for close to half of the total flux recirculation required to balance the dayside reconnection [*Angelopoulos et al.*, 1994; *Schödel et al.*, 2001].

[20] Although the events presented in Figures 2 and 3 all bear close similarities to terrestrial dipolarizations, their spatial and temporal scales are different. The dipolarizations frequently increase the magnetic field strength by 40 nT or more, primarily in the B_z direction, equivalent to a relative increase by a factor of ∼4 over the background magnetotail field strength. A few events recorded dipolarization fields as high as 70 nT. These values can be compared with an average increase of ∼6 nT at Earth [*Lee et al.*, 2012], although terrestrial events with a magnitude of 15–30 nT are frequently reported [e.g., *Runov et al.*, 2009; *Sergeev et al.*, 2009], often equivalent to an increase in the magnetic field strength by a factor of ∼2, although a large variability exists.

[21] For dipolarizations associated with bursty bulk flows, the dipolarization timescale is related to the plasma convection velocity and the width of the dipolarization front. For terrestrial events, this timescale varies between a few and ∼30 s [e.g., *Angelopoulos et al.*, 1992]. The background field tends to be in the neighborhood of 5–10 nT [e.g., *Lee et al.*, 2012], which gives an H^+ ion cyclotron period similar to or slightly shorter than that for the dipolarization events observed at Mercury.

[22] It should be noted, however, that the present analysis concerns only the strongest dipolarization events at Mercury, the properties of which might not adequately describe the average signature, and that the magnitude of the B_z increase is also dependent on the spacecraft location. A general comment concerning the solar wind conditions during these events is that they seem to be observed during relatively weak IMF, and often during periods with a varying B_z component. This observation is in agreement with the conclusions derived from observations during MESSENGER's second and third Mercury flybys that a B_z component varying on the timescale of the Dungey cycle may yield a more dynamic loading–unloading interaction between the solar wind and the magnetosphere than during steady southward IMF [*Slavin et al.*, 2012]. Because of the large time differences between the dipolarizations and the observations of both the inbound and outbound magnetopause and bow shock crossings, however, we cannot determine the IMF conditions at the time of the plasma sheet crossings with certainty.

[23] It has been suggested that BBFs at Earth are coupled to convecting low-entropy plasma-depleted bubbles created by bursts of reconnection in the magnetotail, with additional acceleration provided by the imbalance of the $\mathbf{J} \times \mathbf{B}$ (where $\mathbf{J}$ is current) and plasma pressure forces at the dipolarization front and buoyancy forces due to the low plasma density [e.g., *Pontius and Wolf*, 1990; *Chen and Wolf*, 1999; *Li et al.*, 2011; *Birn et al.*, 2011]. Alternatively, similar dipolarization signatures may also result from kinetic instabilities in the near-Mercury cross-tail current sheet. For example, a spatial inhomogeneity in the magnetic field may feed ballooning and Rayleigh-Taylor

Table 2. Maximum, Intermediate, and Minimum Variance Directions, Eigenvalue Ratios, and α Values for Selected Dipolarization Events[a]

Year	Day	Time (UTC)	Maximum Variance	Intermediate Variance	Minimum Variance	λ_1/λ_2	λ_2/λ_3	α
2011	29 Sep	10:51:31	[−0.19, 0.22, 0.96]	[0.71, 0.70, −0.02]	[−0.67, 0.68, −0.29]	35.7	7.6	−45.2
2011	29 Sep	10:52:09	[−0.24, 0.25, 0.94]	[0.12, 0.97, −0.23]	[−0.96, 0.05, −0.26]	22.9	3.7	−3.1
2011	29 Sep	10:52:27	[−0.54, 0.29, 0.79]	[0.32, −0.80, 0.51]	[−0.78, −0.53, −0.34]	36.9	4.7	34.1
2011	14 Dec	18:28:10	[0.38, 0.28, 0.88]	[0.90, −0.30, −0.30]	[0.18, 0.91, −0.37]	20.3	4.6	78.5
2011	14 Dec	18:28:17	[0.19, 0.29, 0.94]	[0.93, −0.36, −0.07]	[0.32, 0.89, −0.33]	37.1	2.2	70.1
2011	14 Dec	18:30:05	[−0.01, 0.14, 0.99]	[−0.04, 0.99, −0.14]	[1.00, 0.05, 0]	46.8	3.1	2.6
2011	14 Dec	18:30:21	[−0.12, 0.08, 0.99]	[0.04, 1.00, −0.07]	[−0.99, 0.03, −0.12]	77.9	2.7	−1.8
2011	15 Dec	18:04:44	[−0.01, −0.22, 0.98]	[0.17, 0.96, 0.22]	[0.98, −0.17, −0.03]	64.9	4.2	−9.8
2011	26 Dec	13:25:07	[−0.41, 0.33, 0.85]	[−0.40, 0.77, −0.49]	[0.82, 0.54, 0.18]	4.0	28.4	33.2

[a]Positive and negative values of α correspond to dipolarization bubbles passing on the dawnward and duskward side of the spacecraft, respectively.

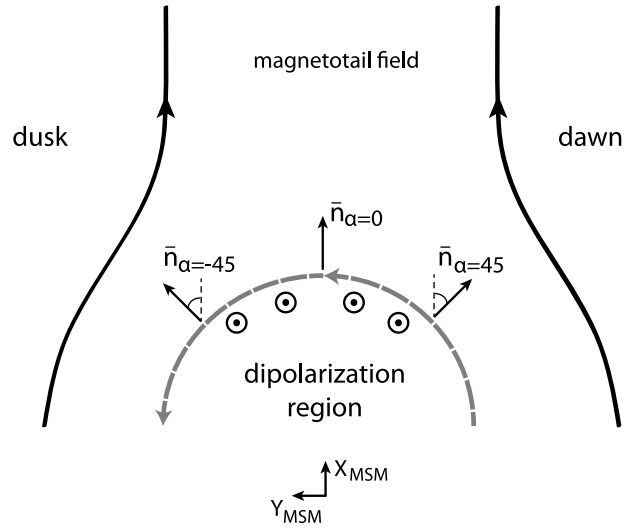

Figure 7. Schematic illustration of an *X–Y* cross-section of a dipolarization region in the magnetotail, north of the cross-tail current sheet. The dashed gray line denotes the current sheet at the boundary of the dipolarization region; arrowheads indicate the direction of the current. The thin black arrows indicate the current-sheet normal directions at $\alpha = -45°$, $\alpha = 0°$, and $\alpha = 45°$, and the thick black lines and circles represent the in-plane and out-of-plane components of the magnetic field, respectively. After *Sergeev et al.* [1996b].

instabilities, leading to localized regions of sunward plasma flow and magnetic field compressions [*Pritchett and Coroniti*, 2010].

[24] Both of these interpretations are intimately connected to regions of enhanced plasma flow and field-aligned current systems. The discontinuity in the gradient and curvature drift currents at the dawn- and duskward edges of such a fast-flowing region leads to charge build-up, polarization, and a field-aligned current system with a planetward current on the dawnward edge of a flow channel and a return current on the duskward edge [e.g., *Pontius and Wolf*, 1990; *Chen and Wolf*, 1993; *Sergeev*, 2004; *Keiling et al.*, 2009; *Pritchett and Coroniti*, 2010; *Birn et al.*, 2011]. At Earth, simultaneous measurements of magnetotail BBFs and their conjugate ionospheric responses have further confirmed the BBF-FAC relationship, and thus their importance in the substorm-like behavior of the magnetotail [e.g., *Angelopoulos et al.*, 1997; *Kauristie et al.*, 2000; *Nakamura et al.*, 2001, 2004; *Grocott et al.*, 2004; *Keiling et al.*, 2009].

4.1. Field-Aligned Current Systems

[25] The observation of dipolarization regions with limited cross-tail extent is an important clue for understanding magnetospheric flux circulation at Mercury. However, the manner in which the associated current systems behave on a larger scale is enigmatic, as the planet's regolith is believed to be highly resistive, allowing little to no current closure through the subsurface. This argument is further strengthened by the lack of FAC signatures in low-altitude regions. This contradiction may partly be resolved by current-carrying Alfvén waves that are reflected at the planetary surface. *Pontius and Wolf* [1990] noted in the terrestrial situation that for high plasma flow velocities in situations where the motion of the dipolarization front during the Alfvén wave reflection time is large compared with the scale of the feature, a stationary FAC cannot be established between the BBF and the ionosphere. For a plasma density of $\sim$7 cm^{-3} in Mercury's plasma sheet and an approximate magnetic field strength of 50 nT, the Alfvén wave velocity is $\sim$400 km/s. As a dipole field line intersecting the equatorial magnetotail at $X = -1.5\ R_M$ has an approximate length of 2 R_M, the reflection timescale for an Alfvén wave launched from the equatorial plane is up to 10 s. Further, for a modest propagation velocity of 200 km/s for the dipolarization front and an X-line located between -1.8 and $-2.8\ R_M$ [*Slavin et al.*, 2012], the dipolarization may transit almost the entire plasma sheet before the return of the reflected wave. This situation can prevent steady state field-aligned current systems from being set up and instead lead to a dynamic system following principles similar to those suggested by *Lyatsky et al.* [2010] for the polar cap, in which a field-aligned current would be allowed to flow due to the fast motion of the plasma in the generator region. How and where the final current closure and Alfvén wave damping may take place is yet unclear. We also note that the estimated Alfvén wave reflection time is close to the average recovery time of the dipolarizations, so current return may play a fundamental role in the timescale of the recovery phase.

4.2. Particle Acceleration

[26] One of the most important consequences of dipolarization fronts in the terrestrial magnetosphere is the non-adiabatic heating and subsequent injection of heavy ions into the ring current region, and we can expect that the quick dipolarizations observed at Mercury may have similar consequences for the ions and electrons in Mercury's plasma sheet. An overview of the gyroperiods for electrons, protons, and a few heavy ion species for typical magnetic fields before and after the dipolarization front is given in Table 3. It is evident that the ion species will experience a non-adiabatic motion, as their cyclotron period is on the order of the dipolarization timescale (H^+ and He^+) or substantially larger (e.g., Ca^+, Na^+). The adiabatic motion of the electrons can be verified through the following inequality [*Delcourt et al.*, 1990], the condition for which seems to be generally satisfied for the dipolarization events described here:

$$\frac{\tau_e \frac{dB}{dt}}{B} \ll 1 \tag{1}$$

where τ_e represents the electron gyroperiod. The electron population will thus primarily experience adiabatic heating (betatron acceleration), with an energy gain on the order of

Table 3. Approximate Gyroperiods for Different Species Before and After the Arrival of a Dipolarization Front

Particle	10 nT Gyroperiod	50 nT Gyroperiod
e^-	3.6 ms	0.7 ms
H^+	6.6 s	1.3 s
He^+	26.2 s	5.2 s
O^+	105 s	21 s
Na^+	151 s	30 s
Ca^+	262 s	52 s

the relative magnetic field increase, i.e., a factor of ~5. Although the electron motion is primarily adiabatic with respect to the first adiabatic invariant, the second adiabatic invariant may not necessarily be conserved, as the bounce period of the electrons is on the order of the dipolarization time frame [*Delcourt et al.*, 2005].

[27] The non-adiabatic heating of ions in Mercury's magnetosphere was analyzed by *Delcourt et al.* [2007] through a particle tracing code. They concluded that the species for which the ion gyroperiod is in close to one-to-one resonance with the dipolarization timescale, primarily H^+ and He^+, could experience an increase in their energy levels by up to two orders of magnitude, whereas heavier species with longer gyroperiods would experience little to no acceleration. The newly energized particles would then quickly drift into the dusk-side magnetosphere, creating a population of highly energized protons on the dusk side of the planet. From a comparison of the main dipolarization timescale of ~1–2 s and the ion cyclotron periods given in Table 3, there is a good match for non-adiabatic heating of H^+, supporting the argument that magnetic field dipolarizations are an important mechanism for proton acceleration at Mercury. However, there are limits to possible accelerations. *Zelenyi et al.* [1990, 2007] derived theoretical estimates of particle heating in Mercury's magnetosphere that predict an upper bound on the proton energy gain of ~60 keV (compared with ~1.6 MeV at Earth) in the acceleration region, and indicate that the acceleration of heavy particles is limited by the small spatial dimensions of the magnetotail.

[28] As mentioned in Section 3, measurements from the XRS and EPS instruments did show the presence of 1–10 keV and higher-energy electrons around the time periods of interest, but no correlations between the particle and magnetic field data could be established. This lack of correlation may be due to a mix of reasons. The 3-s temporal resolution of the EPS instrument may not be able to fully resolve small-scale features at the dipolarization front. Also, the repeated creation of dipolarization events in the magnetotail leads to an almost continuous source of electron acceleration in the magnetotail. Considering the relatively long bounce period of the particles, the observations may thus not necessarily be tied to locally heated electrons at the dipolarization front, but rather to a global nightside population of high-energy plasma.

5. Conclusions

[29] The observations presented here provide strong evidence for dipolarization events in Mercury's magnetic tail, possibly related to plasma flows similar to the bursty bulk flows observed during active periods in the terrestrial magnetotail. The dipolarizations were observed at several occasions in the near-tail plasma sheet, often with several consecutive events during the spacecraft's plasma sheet crossing. The rise time of the dipolarizations was in general less than 2 s, and their lifespan was on the order of 10 s. A detailed analysis of a sub-series of events confirmed that these features are spatially constrained in the cross-tail direction, and that the main dipolarization occurred on the dawnward or duskward side of the spacecraft approximately half of the time for each situation. These results provide insight into the character of the magnetotail unloading process at Mercury and suggest that substorm-like phenomena can develop in Mercury's magnetotail in association with both field-aligned currents and particle acceleration. The swift increase in magnetic field strength at the dipolarization front provides a source for both adiabatic heating of the plasma sheet electron population, albeit on timescales that may not conserve the second adiabatic invariant, and a source for efficient non-adiabatic heating of the plasma sheet protons. Heavier ions are not expected to experience any noticeable heating during the dipolarization.

[30] **Acknowledgments.** The MESSENGER project is supported by the NASA Discovery Program under contracts NAS5-97271 to The Johns Hopkins University Applied Physics Laboratory and NASW-00002 to the Carnegie Institution of Washington. This research was also supported by the NASA Postdoctoral Program at the Goddard Space Flight Center, administered by Oak Ridge Associated Universities through a contract with NASA.

[31] Masaki Fujimoto thanks the reviewers for their assistance in evaluating the paper.

References

Alexeev, I. I., E. S. Belenkaya, S. Y. Bobrovnikov, J. A. Slavin, and M. Sarantos (2008), Paraboloid model of Mercury's magnetosphere, *J. Geophys. Res.*, *113*, A12210, doi:10.1029/2008JA013368.

Alexeev, I. I., et al. (2010), Mercury's magnetospheric magnetic field after the first two MESSENGER flybys, *Icarus*, *209*, 23–39, doi:10.1016/j.icarus.2010.01.024.

Anderson, B. J., M. H. Acuña, D. A. Lohr, J. Scheifele, A. Raval, H. Korth, and J. A. Slavin (2007), The Magnetometer instrument on MESSENGER, *Space Sci. Rev.*, *131*, 417–450, doi:10.1007/s11214-007-9246-7.

Anderson, B. J., C. L. Johnson, H. Korth, M. E. Purucker, R. M. Winslow, J. A. Slavin, S. C. Solomon, R. L. McNutt Jr., J. M. Raines, and T. H. Zurbuchen (2011), The global magnetic field of Mercury from MESSENGER orbital observations, *Science*, *333*, 1859–1862, doi:10.1126/science.1211001.

Andrews, G. B., et al. (2007), The Energetic Particle and Plasma Spectrometer instrument on the MESSENGER spacecraft, *Space Sci. Rev.*, *131*, 523–556, doi:10.1007/s11214-007-9272-5.

Angelopoulos, V., W. Baumjohann, C. F. Kennel, F. V. Coroniti, M. G. Kivelson, R. Pellat, R. J. Walker, H. Lühr, and G. Paschmann (1992), Bursty bulk flows in the inner central plasma sheet, *J. Geophys. Res.*, *97*, 4027–4039, doi:10.1029/91JA02701.

Angelopoulos, V., C. F. Kennel, F. V. Coroniti, R. Pellat, M. G. Kivelson, R. J. Walker, C. T. Russell, W. Baumjohann, W. C. Feldman, and J. T. Gosling (1994), Statistical characteristics of bursty bulk flow events, *J. Geophys. Res.*, *99*, 21,257–21,280, doi:10.1029/94JA01263.

Angelopoulos, V., et al. (1997), Magnetotail flow bursts: Association to global magnetospheric circulation, relationship to ionospheric activity and direct evidence for localization, *Geophys. Res. Lett.*, *24*, 2271–2274, doi:10.1029/97GL02355.

Asano, Y., et al. (2010), Electron acceleration signatures in the magnetotail associated with substorms, *J. Geophys. Res.*, *115*, A05215, doi:10.1029/2009JA014587.

Ashour-Abdalla, M., M. El-Alaoui, M. L. Goldstein, M. Zhou, D. Schriver, R. Richard, R. Walker, M. G. Kivelson, and K.-J. Hwang (2011), Observations and simulations of non-local acceleration of electrons in magnetotail magnetic reconnection events, *Nat. Phys.*, *7*, 360–365, doi:10.1038/nphys1903.

Baker, D. N., J. A. Simpson, and J. H. Eraker (1986), A model of impulsive acceleration and transport of energetic particles in Mercury's magnetosphere, *J. Geophys. Res.*, *91*, 8742–8748, doi:10.1029/JA091iA08p08742.

Baker, D. N., T. I. Pulkkinen, V. Angelopoulos, W. Baumjohann, and R. L. McPherron (1996), Neutral line model of substorms: Past results and present view, *J. Geophys. Res.*, *101*, 12,975–13,010, doi:10.1029/95JA03753.

Baumjohann, W., G. Paschmann, and H. Lühr (1990), Characteristics of high-speed ion flows in the plasma sheet, *J. Geophys. Res.*, *95*, 3801–3809, doi:10.1029/JA095iA04p03801.

Birn, J., R. Nakamura, E. V. Panov, and M. Hesse (2011), Bursty bulk flows and dipolarization in MHD simulations of magnetotail reconnection, *J. Geophys. Res.*, *116*, A01210, doi:10.1029/2010JA016083.

Boardsen, S. A., J. A. Slavin, B. J. Anderson, H. Korth, D. Schriver, and S. C. Solomon (2012), Survey of coherent ~1 Hz waves in Mercury's inner

magnetosphere from MESSENGER observations, *J. Geophys. Res.*, doi:10.1029/2012JA017822, in press.
Chen, C. X., and R. A. Wolf (1993), Interpretation of high-speed flows in the plasma sheet, *J. Geophys. Res.*, *98*, 21,409–21,419, doi:10.1029/93JA02080.
Chen, C. X., and R. A. Wolf (1999), Theory of thin-filament motion in Earth's magnetotail and its application to bursty bulk flows, *J. Geophys. Res.*, *104*, 14,613–14,626, doi:10.1029/1999JA900005.
Christon, S. P., J. Feynman, and J. A. Slavin (1987), Dynamic substorm injections–Similar magnetospheric phenomena at Earth and Mercury, in *Magnetotail Physics*, edited by A. T. Y. Lui, pp. 393–400, Johns Hopkins Univ. Press, Baltimore, Md.
Delcourt, D. C., J. A. Sauvaud, and A. Pedersen (1990), Dynamics of single-particle orbits during substorm expansion phase, *J. Geophys. Res.*, *95*, 20,853–20,865, doi:10.1029/JA095iA12p20853.
Delcourt, D. C., K. Seki, N. Terada, and Y. Miyoshi (2005), Electron dynamics during substorm dipolarization in Mercury's magnetosphere, *Ann. Geophys.*, *23*, 3389–3398, doi:10.5194/angeo-23-3389-2005.
Delcourt, D. C., F. Leblanc, K. Seki, N. Terada, T. E. Moore, and M.-C. Fok (2007), Ion energization during substorms at Mercury, *Planet. Space Sci.*, *55*, 1502–1508, doi:10.1016/j.pss.2006.11.026.
Dungey, J. W. (1961), Interplanetary magnetic fields and the auroral zones, *Phys. Rev. Lett.*, *6*, 47–48, doi:10.1103/PhysRevLett.6.47.
Eraker, J. H., and J. A. Simpson (1986), Acceleration of charged particles in Mercury's magnetosphere, *J. Geophys. Res.*, *91*, 9973–9993, doi:10.1029/JA091iA09p09973.
Grocott, A., T. K. Yeoman, R. Nakamura, S. W. H. Cowley, H. U. Frey, H. Rème, and B. Klecker (2004), Multi-instrument observations of the ionospheric counterpart of a bursty bulk flow in the near-Earth plasma sheet, *Ann. Geophys.*, *22*, 1061–1075, doi:10.5194/angeo-22-1061-2004.
Ho, G. C., R. D. Starr, R. E. Gold, S. M. Krimigis, J. A. Slavin, D. N. Baker, B. J. Anderson, R. L. McNutt Jr., L. R. Nittler, and S. C. Solomon (2011), Observations of suprathermal electrons in Mercury's magnetosphere during the three MESSENGER flybys, *Planet. Space Sci.*, *59*, 2016–2025, doi:10.1016/j.pss.2011.01.011.
Kauristie, K., V. A. Sergeev, M. Kubyshkina, T. I. Pulkkinen, V. Angelopoulos, T. Phan, R. P. Lin, and J. A. Slavin (2000), Ionospheric current signatures of transient plasma sheet flows, *J. Geophys. Res.*, *105*, 10,677–10,690, doi:10.1029/1999JA900487.
Keiling, A., et al. (2009), Substorm current wedge driven by plasma flow vortices: THEMIS observations, *J. Geophys. Res.*, *114*, A00C22, doi:10.1029/2009JA014114.
Kissinger, J., R. L. McPherron, T.-S. Hsu, and V. Angelopoulos (2012), Diversion of plasma due to high pressure in the inner magnetosphere during steady magnetospheric convection, *J. Geophys. Res.*, *117*, A05206, doi:10.1029/2012JA017579.
Korth, H., B. J. Anderson, J. M. Raines, J. A. Slavin, T. H. Zurbuchen, C. L. Johnson, M. E. Purucker, R. M. Winslow, S. C. Solomon, and R. L. McNutt Jr. (2011), Plasma pressure in Mercury's equatorial magnetosphere derived from MESSENGER Magnetometer observations, *Geophys. Res. Lett.*, *38*, L22201, doi:10.1029/2011GL049451.
Lee, D.-Y., H.-S. Kim, S. Ohtani, and M. Y. Park (2012), Statistical characteristics of plasma flows associated with magnetic dipolarizations in the near-tail region of $r < 12\ R_E$, *J. Geophys. Res.*, *117*, A01207, doi:10.1029/2011JA017246.
Li, S.-S., V. Angelopoulos, A. Runov, X.-Z. Zhou, J. McFadden, D. Larson, J. Bonnell, and U. Auster (2011), On the force balance around dipolarization fronts within bursty bulk flows, *J. Geophys. Res.*, *116*, A00I35, doi:10.1029/2010JA015884.
Lyatsky, W., G. V. Khazanov, and J. A. Slavin (2010), Alfven wave reflection model of field-aligned currents at Mercury, *Icarus*, *209*, 40–45, doi:10.1016/j.icarus.2009.11.039.
Nakamura, R., W. Baumjohann, R. Schödel, M. Brittnacher, V. A. Sergeev, M. Kubyshkina, T. Mukai, and K. Liou (2001), Earthward flow bursts, auroral streamers, and small expansions, *J. Geophys. Res.*, *106*, 10,791–10,802, doi:10.1029/2000JA000306.
Nakamura, R., et al. (2004), Spatial scale of high-speed flows in the plasma sheet observed by Cluster, *Geophys. Res. Lett.*, *31*, L09804, doi:10.1029/2004GL019558.
Ohtani, S., M. A. Shay, and T. Mukai (2004), Temporal structure of the fast convective flow in the plasma sheet: Comparison between observations and two-fluid simulations, *J. Geophys. Res.*, *109*, A03210, doi:10.1029/2003JA010002.
Pontius, D. H., Jr., and R. A. Wolf (1990), Transient flux tubes in the terrestrial magnetosphere, *Geophys. Res. Lett.*, *17*, 49–52, doi:10.1029/GL017i001p00049.
Pritchett, P. L., and F. V. Coroniti (2010), A kinetic ballooning/interchange instability in the magnetotail, *J. Geophys. Res.*, *115*, A06301, doi:10.1029/2009JA014752.
Raines, J. M., J. A. Slavin, T. H. Zurbuchen, G. Gloeckler, B. J. Anderson, D. N. Baker, H. Korth, S. M. Krimigis, and R. L. McNutt Jr. (2011), MESSENGER observations of the plasma environment near Mercury, *Planet. Space Sci.*, *59*, 2004–2015, doi:10.1016/j.pss.2011.02.004.
Raj, A., T. Phan, R. P. Lin, and V. Angelopoulos (2002), Wind survey of high-speed bulk flows and field-aligned beams in the near-Earth plasma sheet, *J. Geophys. Res.*, *107*(A12), 1419, doi:10.1029/2001JA007547.
Runov, A., V. Angelopoulos, M. I. Sitnov, V. A. Sergeev, J. Bonnell, J. P. McFadden, D. Larson, K.-H. Glassmeier, and U. Auster (2009), THEMIS observations of an earthward-propagating dipolarization front, *Geophys. Res. Lett.*, *36*, L14106, doi:10.1029/2009GL038980.
Runov, A., V. Angelopoulos, X.-Z. Zhou, X.-J. Zhang, S. Li, F. Plaschke, and J. Bonnell (2011), A THEMIS multicase study of dipolarization fronts in the magnetotail plasma sheet, *J. Geophys. Res.*, *116*, A05216, doi:10.1029/2010JA016316.
Schmid, D., M. Volwerk, R. Nakamura, W. Baumjohann, and M. Heyn (2011), A statistical and event study of magnetotail dipolarization fronts, *Ann. Geophys.*, *29*, 1537–1547, doi:10.5194/angeo-29-1537-2011.
Schödel, R., W. Baumjohann, R. Nakamura, V. A. Sergeev, and T. Mukai (2001), Rapid flux transport in the central plasma sheet, *J. Geophys. Res.*, *106*, 301–313, doi:10.1029/2000JA900139.
Schriver, D., et al. (2011), Quasi-trapped particle population around Mercury, *Geophys. Res. Lett.*, *38*, L23103, doi:10.1029/2011GL049629.
Sergeev, V. A. (2004), Bursty bulk flows and their ionospheric footprints, in *Multiscale Processes in the Earth's Magnetosphere: From Interball to Cluster*, edited by J.-A. Sauvaud and Z. Němeček, pp. 289–306, Kluwer Acad., Dordrecht, Netherlands, doi:10.1007/1-4020-2768-0_16.
Sergeev, V. A., W. Lennartsson, R. Pellinen, M. Vallinkoski, and N. I. Fedorova (1990), Average patterns of precipitation and plasma flow in the plasma sheet flux tubes during steady magnetospheric convection, *Planet. Space Sci.*, *38*, 355–363, doi:10.1016/0032-+0633(90)90101-U.
Sergeev, V. A., R. J. Pellinen, and T. I. Pulkkinen (1996a), Steady magnetospheric convection: A review of recent results, *Space Sci. Rev.*, *75*, 551–604, doi:10.1007/BF00833344.
Sergeev, V. A., V. Angelopoulos, J. T. Gosling, C. A. Cattell, and C. T. Russell (1996b), Detection of localized, plasma-depleted flux tubes or bubbles in the midtail plasma sheet, *J. Geophys. Res.*, *101*, 10,817–10,826, doi:10.1029/96JA00460.
Sergeev, V., V. Angelopoulos, S. Apatenkov, J. Bonnell, R. Ergun, R. Nakamura, J. McFadden, D. Larson, and A. Runov (2009), Kinetic structure of the sharp injection/dipolarization front in the flow-braking region, *Geophys. Res. Lett.*, *36*, L21105, doi:10.1029/2009GL040658.
Sigsbee, K., J. A. Slavin, R. P. Lepping, A. Szabo, M. Øieroset, M. L. Kaiser, M. J. Reiner, and H. J. Singer (2005), Statistical and superposed epoch study of dipolarization events using data from Wind perigee passes, *Ann. Geophys.*, *23*, 831–851, doi:10.5194/angeo-23-831-2005.
Slavin, J. A., et al. (2008), Mercury's magnetosphere after MESSENGER's first flyby, *Science*, *321*, 85–89, doi:10.1126/science.1159040.
Slavin, J. A., et al. (2009), MESSENGER observations of magnetic reconnection in Mercury's magnetosphere, *Science*, *324*, 606–610, doi:10.1126/science.1172011.
Slavin, J. A., et al. (2010), MESSENGER observations of extreme loading and unloading of Mercury's magnetic tail, *Science*, *329*, 665–668, doi:10.1126/science.1188067.
Slavin, J. A., et al. (2012), MESSENGER and Mariner 10 flyby observations of magnetotail structure and dynamics at Mercury, *J. Geophys. Res.*, *117*, A01215, doi:10.1029/2011JA016900.
Solomon, S. C., et al. (2001), The MESSENGER mission to Mercury: Scientific objectives and implementation, *Planet. Space Sci.*, *49*, 1445–1465, doi:10.1016/S0032-0633(01)00085-X.
Sonnerup, B. U. Ö., and M. Scheible (1998), Minimum and maximum variance analysis, in *Analysis Methods for Multi-Spacecraft Data*, *ISSI Sci. Rep. Ser.*, vol. 1, edited by G. Paschmann and P. Daly, pp. 185–220, Eur. Space Agency, Noordwijk, Netherlands.
Sundberg, T., S. A. Boardsen, J. A. Slavin, B. J. Anderson, H. Korth, T. H. Zurbuchen, J. M. Raines, and S. C. Solomon (2012), MESSENGER orbital observations of large-amplitude Kelvin-Helmholtz waves at Mercury's magnetopause, *J. Geophys. Res.*, *117*, A04216, doi:10.1029/2011JA017268.
Uritsky, V. M., J. A. Slavin, G. V. Khazanov, E. F. Donovan, S. A. Boardsen, B. J. Anderson, and H. Korth (2011), Kinetic-scale magnetic turbulence and finite Larmor radius effects at Mercury, *J. Geophys. Res.*, *116*, A09236, doi:10.1029/2011JA016744.
Zelenyi, L. M., J. G. Lominadze, and A. L. Taktakishvili (1990), Generation of the energetic proton and electron bursts in planetary magnetotails, *J. Geophys. Res.*, *95*, 3883–3891, doi:10.1029/JA095iA04p03883.
Zelenyi, L., M. Oka, H. Malova, M. Fujimoto, D. Delcourt, and W. Baumjohann (2007), Particle acceleration in Mercury's magnetosphere, *Space Sci. Rev.*, *132*, 593–609, doi:10.1007/s11214-007-9169-3.